Energy Conversion and Management 164 (2018) 198–209

Contents lists available at ScienceDirect

Energy Conversion and Management

journal homepage: www.elsevier.com/locate/enconman

Influence of microcapsule size and shell polarity on thermal and mechanical properties of thermoregulating geopolymer concrete for passive building applications

Vinh Duy Cao[a,b], Shima Pilehvar[a,c], Carlos Salas-Bringas[b], Anna M. Szczotok[a,d], Luca Valentini[e], Manuel Carmona[d], Juan F. Rodriguez[d], Anna-Lena Kjøniksen[a,*]

[a] Faculty of Engineering, Østfold University College, N-1757 Halden, Norway
[b] Faculty of Science and Technology, Norwegian University of Life Sciences, N-1432 Ås, Norway
[c] Department of Material Engineering and Manufacturing, Technical University of Cartagena, Cartagena, Murcia, Spain
[d] Department of Chemical Engineering, University of Castilla – La Mancha, 13004 Ciudad Real, Spain
[e] Department of Geosciences, University of Padua, 35131 Padua, Italy

ARTICLE INFO

Keywords:
Microencapsulated phase change materials
Geopolymer concrete
Thermal diffusivity
Energy efficiency
Thermal conductivity

ABSTRACT

Microencapsulated phase change materials (MPCM) were added to geopolymer concrete (GPC) for utilization as a thermal energy storage concrete for passive building applications. Three different MPCM were compared to examine the influence of the hygroscopic nature of the MPCM shell, the PCM core/polymer shell ratio, and the MPCM size on the microstructure, thermal properties and compressive strength of GPC. The combination of a hygroscopic nature of the polymer shell, a high core/shell ratio, and a small MPCM size were found to improve the interface bonds between microcapsules and the GPC matrix, increase the energy storage capacity of GPC, and results in a good dispersion of MPCM in the GPC matrix. After adding 5.2 wt% MPCM to GPC, the power consumption for stabilizing the indoor temperature at 23 °C may be reduced by up to 18.5 ± 0.3% for GPC containing PS-DVB/RT27 (paraffin Rubitherm®RT27 core and a shell of polystyrene cross-linked with divinylbenzene), 20.1 ± 0.7% for GPC containing PMMA/PCM26 (paraffin mixture core with a crosslinked polymethyl methacrylate shell) and 25.9 ± 0.3% for GPC containing MF/PCM24 (paraffin mixture core with a melamine–formaldehyde polymer shell). Adding MPCM to GPC induces a higher amount of air pockets, which weaken the compressive strength. Unfortunately, the same parameters that are advantageous for reducing the energy consumption also results in a greater decline of the compressive strength. The compressive strength is further reduced when the microcapsule core is in its liquid state. However, the compressive strength still satisfies the mechanical European regulation (EN 206-1, compressive strength class C20/25) for concrete applications, except for GPC containing 5.2 wt% of MF/PCM24.

1. Introduction

With approximately 40% of the total global energy consumption contributed by buildings, reducing the energy consumption for buildings plays a key role for reducing global warming [1,2]. In order to reduce the huge energy consumption of buildings, improved construction techniques and advanced material technology are required. Concrete-based materials are among the most used materials for building applications. With their high mechanical strength and the possibility of changing the properties by varying the concrete recipe, concrete can work not only as a structural material but also as a functional material for thermal energy storage. The energy storage capacity of concrete can be enhanced by integrating microencapsulated phase change materials (MPCM). MPCM can store and release large amounts of energy during the phase transition. This is a promising technology for improving the energy efficiency of buildings, with reduced power consumption for heating and cooling [3–9]. Due to the low thermal conductivity of MPCM and an enhanced porosity, the thermal conductivity of concrete is decreased after addition of MPCM [5]. The decline in the compressive strength of concrete is the main drawback of MPCM addition [3–6]. The destruction of microcapsules during the mixing process might be the reason for the reduction of the compressive strength [3]. The soft nature of MPCM may weaken the concrete [5], and a complete cement hydration may be prevented due to the hygroscopic nature of the

* Corresponding author.
E-mail address: anna.l.kjoniksen@hiof.no (A.-L. Kjøniksen).

https://doi.org/10.1016/j.enconman.2018.02.076
Received 7 December 2017; Received in revised form 1 February 2018; Accepted 22 February 2018

MPCM [6]. In addition, the higher porosity after MPCM addition is probably contributing to the reduced strength [3,5,7].

Most studies of including MPCM in concrete structures are based on Portland cement concrete [3–9]. However, the high amount of CO_2 emission from production of Portland cement is a drawback of utilizing this type of concrete [10]. It is therefore a great advantage to replace Portland cement concrete by more environmentally friendly construction materials such as geopolymer concrete. Geopolymer is synthesized by alkali activation of materials rich in silica and alumina (from industrial waste materials such as fly ash (FA), coal ash, rice-husk ash, red mud and ground granulated blast furnace slag (GGBFS)) [11–14]. Using geopolymer as an alternative binder for concrete can greatly reduce the CO_2 emission from the cement industry. A few studies have examined integration of MPCM to geopolymer concrete [5,7], with promising results for improving the energy efficiency of buildings. It was found that the higher porosity after adding microcapsules contributes to the improvement of the thermal properties and the reduction of the compressive strength of geopolymer concrete. However, the effect of the MPCM properties (hygroscopic nature of the polymer shell, size of the microcapsules, storage heat capacity) on the thermal and mechanical properties of geopolymer concrete was not investigated in previous studies. In addition, it is important to evaluate the effect of the PCM state (solid or liquid) on the compressive strength of concrete.

In the current study, geopolymer concrete is employed as the concrete-based material for integration of microencapsulated phase change materials. Three kinds of microcapsules with variation of polymer shells, heat storage capacity and size were utilized to explore the influence on the microstructure, thermal, and mechanical properties of geopolymer concrete. The effects of the hygroscopic nature of MPCM and different PCM states were given special attention, as previous knowledge within this field is very limited. The effect of MPCM on the energy efficiency of buildings was estimated by determining the power consumption and power reduction of a heating and cooling system.

2. Experimental

2.1. Materials

Three different kinds of microcapsules were utilized. PS-DVB/RT27 was produced by a suspension polymerization process [15]. The MPCM are composed of a paraffin Rubitherm®RT27 core coated with a PS-DVB (polystyrene cross-linked with divinylbenzene) shell. PMMA/PCM26 (Micronal DS-5038X, BASF, Germany) has a core which is a paraffin mixture and highly crosslinked polymethyl methacrylate (PMMA) shell, with a core/shell ratio of 7:3 [16]. MF/PCM24 (Microtek MPCM24D) has a paraffin mixture core and melamine-formaldehyde polymer shell (MF). The ratio between the paraffin core and polymer shell is 9:1 [17]. Table 1 summarizes the characteristics of the three MPCMs.

Geopolymer concrete containing microencapsulated phase change materials (MPCM-GPC) was fabricated by mixing class F fly ash (FA) (Norcem, Germany) (density = 2.26 ± 0.02 g/cm^3), ground granulated blast furnace slag (GGBFS) (Cemex, Germany) (density = 2.85 ± 0.02 g/cm^3), sand (Gunnar Holth and Skolt Pukkverk AS, Norway) (density of 2.7 g/cm^3), aggregates with an average size of approximately 10 mm (Gunnar Holth and Skolt Pukkverk AS, Norway) (density of 2.6 g/cm^3), retarder (FLUBE OS 39, Bozzetto Group, Italy) (density of 1.2 g/cm^3), an alkaline activator solution, and MPCM. The sand and aggregates were dried before use. The chemical composition of FA and GGBFS were obtained by X-ray Fluorescence (XRF) and is summarized in Table 2. Based on a previous study [19], the alkaline activator solution was mixed at a ratio of 1.5 of a sodium silicate solution (density = 1.93 g/cm^3, 35 wt% solid) and 14 M NaOH (560 g/L). Accordingly, $m_{Na2SiO3(aq)}$ = 120 g, and $m_{NaOH(aq)}$ = 80 g. Fresh GPC possesses a poor workability due to the high geopolymerization reaction rate, which has a negative effect on the integration of MPCM into GPC [5,7]. Therefore, a chemical admixture was utilized to improve the workability of the concrete and to facilitate a better distribution of MPCM in the GPC matrix. A naphthalene based retarder was selected due to its high effectiveness with geopolymer concrete containing fly ash class F [20–22].

Table 3 summarizes the composition of geopolymer concrete containing MPCM (MPCM-GPC). For the recipe, a 1 L mix design was obtained from previous studies [7,19]. To keep a constant volume, the sand was replaced by MPCM at the same volume percentage (see supporting document [18] for details). However, the MPCM content is calculated as a wt.% of the total concrete sample, for a clearer comparison of the energy reduction. The mixture was prepared by weighting the components. In order to minimize the effect of shear during the mixing process, MPCM was mixed into GPC during the final step. For more information about the mixing process and recipe, see Pilehvar et al. [7,19].

PCM was incorporated into GPC at 0, 1.3, 2.6 and 5.2 wt%. The concentration of MPCM was limited to 5.2 wt% since higher concentrations of MPCM resulted in too low workability of the geopolymer concrete. After mixing, MPCM-GPC were cast into molds at a size of 200 × 200 × 25 mm (for the thermal test) and 100 × 100 × 100 mm (for the compressive strength test). The samples were pre-cured at room temperature (20 °C) for 24 h. The samples were then demolded and kept in water at room temperature (20 °C) for 28 days to reach a fully cured state. Before conducting the thermal test, the fully cured samples were dried in an oven at 40 °C until the sample weight remained unchanged.

Table 1
The fundamental data of the microencapsulated phase change materials.

MPCM name	Density (g/cm^3)	Melting point* (°C)	Latent heat* (J/g)	Core/shell ratio	Refs.
PS-DVB/RT27	0.9	24.9	100	11:9	[15]
PMMA/PCM26	0.9	24.7	110	7:3	[16]
MF/PCM24	0.9	21.9	154	9:1	[17]

* The melting point and latent heat were determined by differential scanning calorimetry (DSC) (see Supporting document [18] for details).

2.2. Scanning electron microscopy

The surface morphology and the micro structure of the microcapsules (powder form) were obtained by Scanning electron microscopy (SEM) (Quanta FEG-250, Spain). For MPCM-GPC, the fractured surfaces of samples containing 2.6 wt% of MPCM were investigated using a Zeiss EVO50 EP Scanning electron microscope (Norway).

2.3. X-ray micro-tomography

The internal microstructure of GPC containing microcapsules were investigated using X-ray tomography. The X-ray micro-tomography cross-sectional slices of cylindrical samples were obtained using a Skyscan 1172 CT scanner (Bruker) with 80 kV incident radiation, 124 μA source current, 750 ms exposure time per frame and 0.3° rotation step. Tomographic reconstruction was performed using the Feldkamp algorithm [23] and the final pixel size was 6 μm. The samples were made in cylindrical form (1 cm diameter and 1 cm height) from completely curing GPC without MPCM and containing 2.6 wt% of microcapsules (PS-DVB/RT27, PMMA/PCM26 and MF/PCM24).

2.4. Size distribution of MPCM

Low Angel Laser Light Scattering (LALLS) laser diffraction using a Malvern Mastersizer 2000 (Malvern Instruments Ltd., Malvern, UK) equipped with a Scirocco 2000 unit for analyzing dispersions of the particles in air was employed to determine the size distribution of MPCM.

Table 2
Chemical composition of fly ash (FA) and ground granulated blast furnace slag (GGBFS).

Chemical	Al_2O_3	SiO_2	CaO	Fe_2O_3	MgO	K_2O	TiO_2	Na_2O	P_2O_5	SO_3	SrO	CO_2
FA (wt.%)	23.15	50.83	6.87	6.82	1.70	2.14	1.01	1.29	1.14	1.24	0.19	3.07
GGBFS (wt.%)	10.30	34.51	42.84	0.60	7.41	0.52	0.66	0.40	0.02	1.95	0.05	0.30

Table 3
Composition of geopolymer concretes.

MPCM (wt.%)	Alkaline solution (g)	Water (g)	FA* (g)	GGBFS** (g)	Sand (g)	Aggregate (g)	Retarder (g)	MPCM (g)
0	200	50	300	200	871.2	851.7	5	0
1.3	200	50	300	200	784.1	851.7	5	30
2.6	200	50	300	200	696.9	851.7	5	63
5.2	200	50	300	200	522.7	851.7	5	117

* FA: Flyash.
** GGBFS: Ground granulated blast-furnace slag.

2.5. Density and porosity

The density and open porosity of concrete samples were respectively determined by EN 12390-7 (Eq. (1)) [24] and ASTM C1202-12 (Eq. (2)) [25,26].

$$\rho = \frac{m_d}{V} \tag{1}$$

$$Open\ Porosity(\%) = \frac{m_s - m_d}{m_s - m_b} \times 100 \tag{2}$$

where ρ is the dry density of the sample, V is the volume of the sample, and m_d, m_b and m_s are oven-dried weight, the buoyant mass of the saturated sample in water and the mass of the saturated sample in air, respectively.

2.6. Trapped water content

The ability of microcapsules to trap water was determined to compare the polarity of the microcapsules polymer shell. 5.0 ± 0.1 g of each type of microcapsules were immersed in 50 ml of alkaline solution at room temperature (20 °C). After 24 h, the dispersion of microcapsules in alkaline solution was placed into filter test tubes (0.45 μm filter membrane) and centrifuged at 4500 rpm for 5 min (Mega Star 1.6R) to separate the microcapsules from the alkaline solution. The remaining water trapped on the microcapsules were determined utilizing a moisture analyzer (MB 64M-VWR, Italy). The temperature for this test was set at 70 °C. The final trapped water can be obtained after subtracting the water content of the initial microcapsules, which were also determined by the moisture analyzer.

2.7. Thermal properties

The thermal properties of concrete containing MPCM such as the thermal conductivity, the specific heat capacity and the latent heat was determined by the guarded hot plates method [5,27,28]. The sample was sandwiched between two aluminum plate heat exchangers which were connected to thermal regulated baths that define the thermal conditions. In order to minimize the heat transfer from the lateral side face of the samples into the external ambient conditions, a 40 mm thick polyethylene expanded foam (PEF) is used to cover the sample. Accordingly, the heat transfer through the sample can be calculated assuming one-dimensional thermal condition. The temperature variations and heat fluxes through sample during testing were recorded by heat flux sensors (Captecv, France) and T-type thermocouples (OMEGA, US) via a multichannel multimeter (LR8410-20 Hioki, Japan).

2.7.1. Thermal conductivity

The conductivity of the sample is defined according to the European standard EN-12667.

In order to determine the thermal conductivity of concrete containing MPCM, the temperature on the top and bottom aluminum plate heat exchanger were set at $T_{Al\text{-}top}$ and $T_{Al\text{-}bot}$ until a thermal steady state was reached. For solid thermal conductivity determination, $T_{Al\text{-}top}$ and $T_{Al\text{-}bot}$ are set at 5 and 10 °C while 45 and 50 °C are utilized to calculate the liquid thermal conductivity of MPCM-concrete.

The thermal conductivity of the sample in liquid state and solid state of PCM was determined by [5]:

$$k = \frac{\varphi d}{(T_{top} - T_{bottom})} \tag{3}$$

where d is the thickness of the sample. In these experiments the dimension of the concrete samples is d = 25 ± 1 mm. T_{top} and T_{bottom} are the temperature on the top face and bottom face of concrete sample while φ is the average heat fluxes on both faces of concrete sample.

2.7.2. Specific heat capacity/latent heat

In order to determine the specific heat capacity and the latent heat of the concrete containing MPCM, the temperature of both aluminum plate heat exchangers was raised from 5 °C to 45 °C. For this test, the heating rate was set at 10 °C/hour. The heat flux sensors and thermocouples were used to record the heat fluxes (φ) and temperature on both faces of the sample during the test. The specific heat capacity of concrete containing MPCM samples as a function of temperature can be determined by [5,29]:

$$C_p(\mathrm{T}) = \frac{A\varphi(\mathrm{T})}{m\frac{dT}{dt}} \tag{4}$$

Accordingly, the solid specific heat capacity, $C_{p\text{-}solid}$ (below the melting range of PCM) and the liquid specific heat capacity, $C_{p\text{-}liquid}$ (above the melting range of PCM) were estimated as the average value of $C_p(T)$ in the temperature range of 10–15 °C and 35–40 °C, respectively.

The latent heat was calculated in the temperature range of 10–35 °C by Eq. (5) [29] using OriginPro 2016 Sr2.

$$\Delta H = \frac{A}{m}\left(\int_{T1}^{T2} \varphi(T)dT\right) - C_{p-ave}\cdot(T_2 - T_1) \tag{5}$$

where $C_{p\text{-}ave} = (C_{p\text{-}solid} + C_{p\text{-}liquid})/2$ is the average specific heat capacity, ΔH is the latent heat. T_1 = 10 °C and T_2 = 35 °C. A = 400 cm^2 is the area of the sample.

2.7.3. Thermal diffusivity

Because the thermal conductivity and heat storage capacity (specific

heat capacity and latent heat) are inherent capacities of the materials, it is important to reveal their effect on the heat transfer process and on the energy consumption of the heating/cooling system to maintain a constant indoor temperature.

Thermal diffusivity is used to estimate the rate of heat transfer through a material. It also provides a relation between the thermal conductivity and heat storage capacity on the energy performance of building materials. The thermal diffusivity (α) is dependent on the thermal conductivity, the specific heat capacity and the density (ρ) [30]:

$$\alpha(T) = \frac{k_{ave}}{\rho C_p(T)} \tag{6}$$

where $k_{ave} = (k_{solid} + k_{liquid})/2$ is the average thermal conductivity. The average is used since there is little difference between the thermal conductivity of samples where is PCM in a solid or liquid state (see Section 3.3)

2.8. Energy saving aspect

To investigate the effect of microcapsules on the thermal performance (energy saving aspect) of geopolymer concrete, a thermal system was set up as illustrated in Fig. 1.

A small test room was made from a 50 mm of polyethylene expanded foam (PEF) panels for thermal insulation and has inner dimensions of 600 × 800 × 600 mm (Fig. 1). The concrete sample (200 × 200 × 50 mm) was inserted in a rectangular hole of 200 × 200 mm located in the middle of the top insulation panel of the box. The test room was placed inside an environmental chamber to mimic the outdoor environmental temperature variations. The simulated indoor temperature (T_{room}) was set at 23 °C throughout the experiment using a Laird temperature regulator (AA150-Laird Technologies). To mimic outdoor conditions, the outdoor temperature T_{out} was imposed as a sinusoidal function of time using an environmental chamber (VT^3 4250, Vötsch, Germany):

$$T_{out}(t) = \frac{T_{max} + T_{min}}{2} + \frac{T_{max} - T_{min}}{2}\sin\left(\frac{\pi}{43200}t - \frac{2\pi}{3}\right) \tag{7}$$

where T_{max} = 40 °C and T_{min} = 10 °C are the maximum and minimum outdoor temperatures during a day, respectively. The maximum outdoor temperature T_{max} were set at 14:00.

During the initial stage, both indoor temperature and outdoor temperature were set at 23 °C for 2 h to reach a steady-state condition. After that, the outdoor temperature cycles (Eq. (7)) were applied and run for 72 h to determine the thermal performance of the concrete samples and the repeatability of the measurements.

The temperature and heat fluxes on both surfaces of the sample were recorded by using thermocouples and heat flux sensors to measure heat losses towards the simulated indoor environment during the testing process.

It is assumed that there is no heat transfer through the insulation panels of the box. Accordingly, the total energy supplied to the heating/cooling system to maintain the simulated indoor temperature at 23 °C within one day can be calculated as the sum of the heating power consumption (the indoor surface temperature < T_{room}) and the cooling power consumption (the indoor surface temperature > T_{room}):

$$P = \frac{\int_{t_{ini}}^{t_{end}} |\varphi_{indoor}| dt}{3600 \cdot 10^3} \tag{8}$$

where φ_{indoor} is the heat flux on the simulated indoor side of the sample, t_{ini} and t_{end} are the initial time and end time of the thermal cycle.

The power reduction Pr was defined as:

$$Pr = \frac{P_{GPC} - P_{MPCM-GPC}}{P_{GPC}} \cdot 100\% \tag{9}$$

where P_{GPC} and $P_{MPCM\text{-}GPC}$ are the power consumption of the heating and cooling system working within one day for geopolymer concrete without MPCM and with MPCM, respectively.

2.9. Compressive strength test

The effect of different kinds of microcapsules and their concentration on the compressive strength of geopolymer concrete were investigated. An Alpha 3-3000 system (Form + Test Seidner&Co.GmbH) was employed to determine the compressive strength of MPCM-GPC

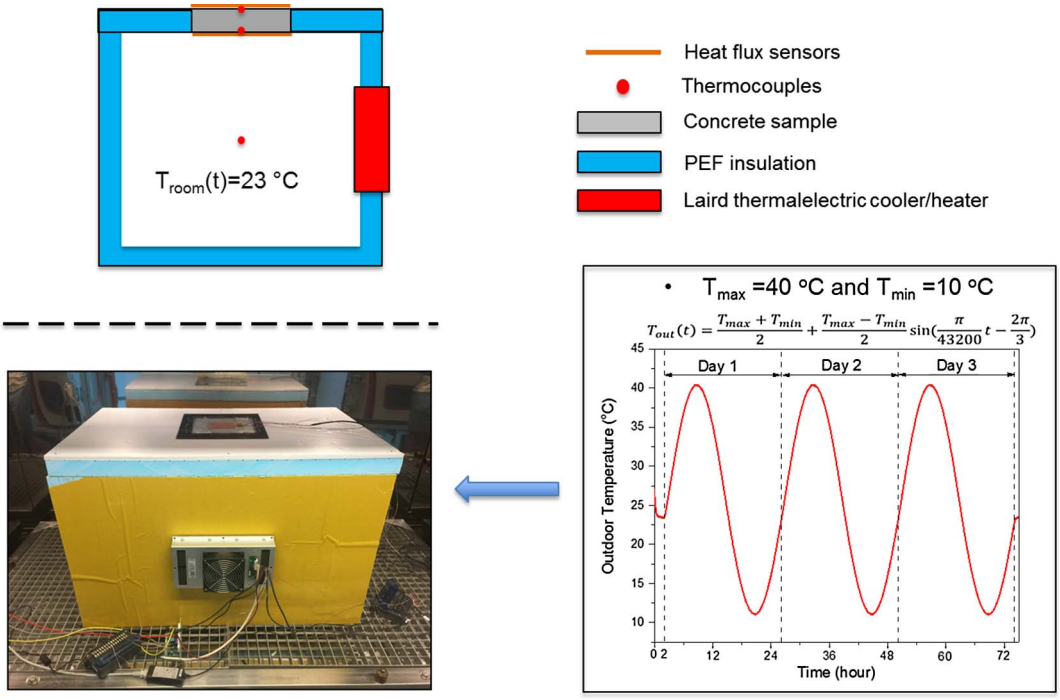

Fig. 1. The thermal performance testing system with sketch of cross-section of the system and the simulated outdoor temperature profile.

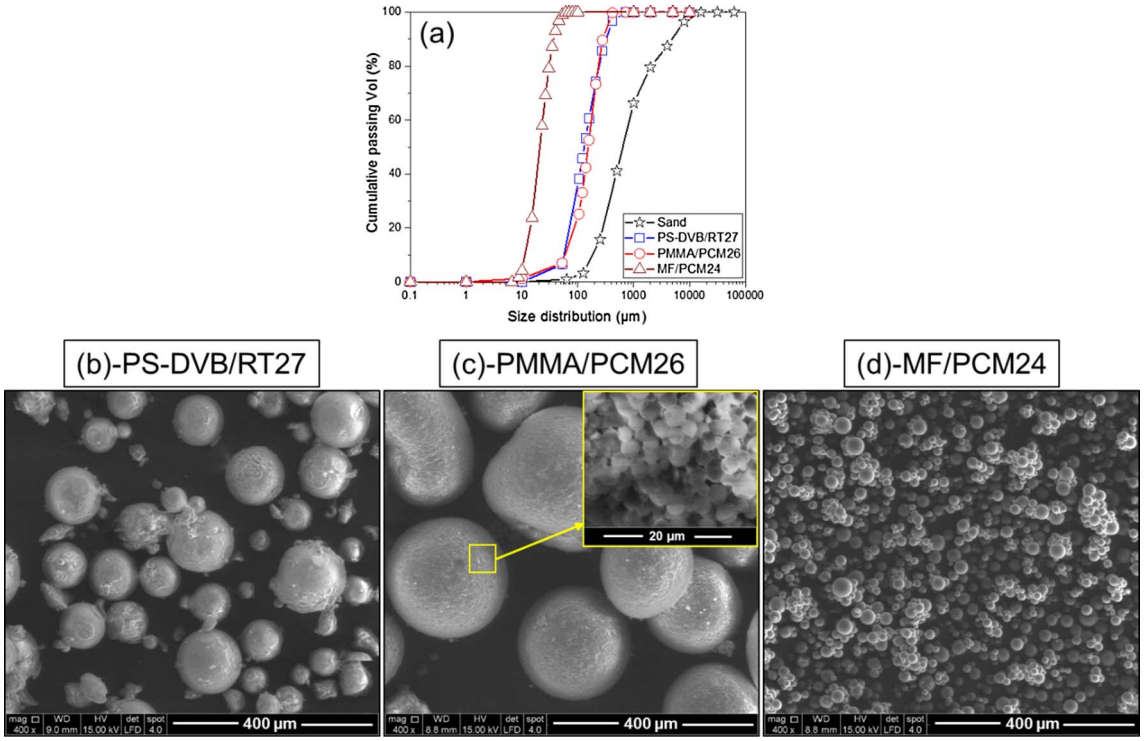

Fig. 2. (a) The size (diameter) distribution of the PS-DVB/RT27, PMMA/PCM26, MF/PCM24 microcapsules and sand, and SEM images of (b) PS-DVB/RT27, (c) PMMA/PCM26 and (d) MF/PCM24. The insert plot (c) shows the single PMMA/PCM26 microcapsules.

samples based on EN 12390-3. In addition, the measurement was conducted at different temperatures including 20 °C (below the melting range) and 40 °C (above the melting range) to examine effect of temperature on the compressive strength of MPCM-GPC samples. The cubes were left in the room for 3 h to remove free water before they were tested at 20 °C. For the test at 40 °C, the temperature of the compressive strength machine was kept at 40 °C by thermal insulation combined with utilization of a temperature regulating incubator connected by an isolated tube. Before the compressive strength test, cubes were kept in room temperature (20 °C) for 3 h to remove free water, followed by storage in a heating chamber at 40 °C for 12 h to obtain a uniform temperature through the whole samples, immediately afterward the cubes were tested. Three cubes were tested for each sample.

3. Results and discussion

Fig. 2 shows size distribution of the microcapsules and the sand, and SEM images of the microcapsules. As is evident from the SEM images, the microcapsules exhibit a spherical shape. They have a diameter in the range of 10–100 μm for PS-DVB/RT27; 1–3 μm for PMMA/PCM26 and 10–30 μm for MF/PCM24. However, all of them have a strong tendency to form agglomerated structures, especially PMMA/PCM26 (Fig. 2c). The size distribution of the agglomerated microcapsules is shown in Fig. 2a. The agglomerated microcapsules have a diameter in the range between 10 and 1000 μm for PS-DVB/RT27, 0.1–800 μm for PMMA/PCM26 and 0.1–100 μm for MF/PCM24. The mean agglomerated microcapsules diameter at 50% in the cumulative distribution (D_{50}) is 130 μm for PS-DVB/RT27, 155 μm for PMMA/PCM26 and 21 μm for MF/PCM24, which is smaller than the size of sand (D_{50} = 640 μm). This difference may have an important impact on the physical properties of the concrete samples.

Fig. 3 presents the trapped water of the microcapsules after immersion for 24 h in an alkaline solution (corresponding to the alkaline solution used in the geopolymer). PS-DVB/RT27 traps less water than PMMA/PCM26 and MF/PCM24. This is reasonable considering the difference in the chemical structures of the polymer shells of the

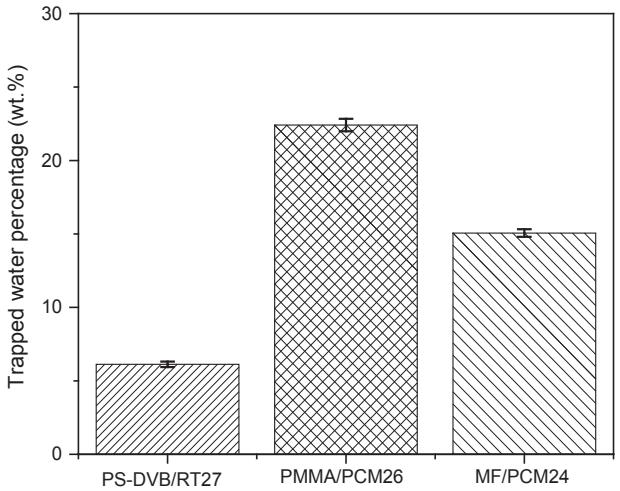

Fig. 3. The trapped water of microcapsules after immersion in an alkaline solution at room temperature (20 °C) for 24 h.

microcapsules. As can be seen from Fig. 4, PS-DVB contains non-polar functional groups (phenyl functional groups) while the functional groups PMMA (ester functional groups) and MF (amine functional groups) are more polar. The existence of polar functional groups renders the polymer shell more compatible with water, causing a higher amount of water to adsorb on the microcapsules.

Fig. 3 also illustrates that PMMA/PCM26 traps more water than MF/PCM24. Accordingly, at alkaline conditions PMMA/PCM26 and MF/PCM24 can trap approximately 22.4 ± 0.4 and 15.1 ± 0.3% of water, respectively. Both the difference in the functional groups (Fig. 4) and the size of the microcapsules (Fig. 2) can contribute to this difference. Although PMMA/PCM26 exists as agglomerated structures with a larger size than MF/PCM24, the single PMMA/PCM26 size (1–3 μm) is approximately 10 times smaller than MF/PCM24 (Fig. 2). After immersing in an alkaline solution for 24 h, the solution can

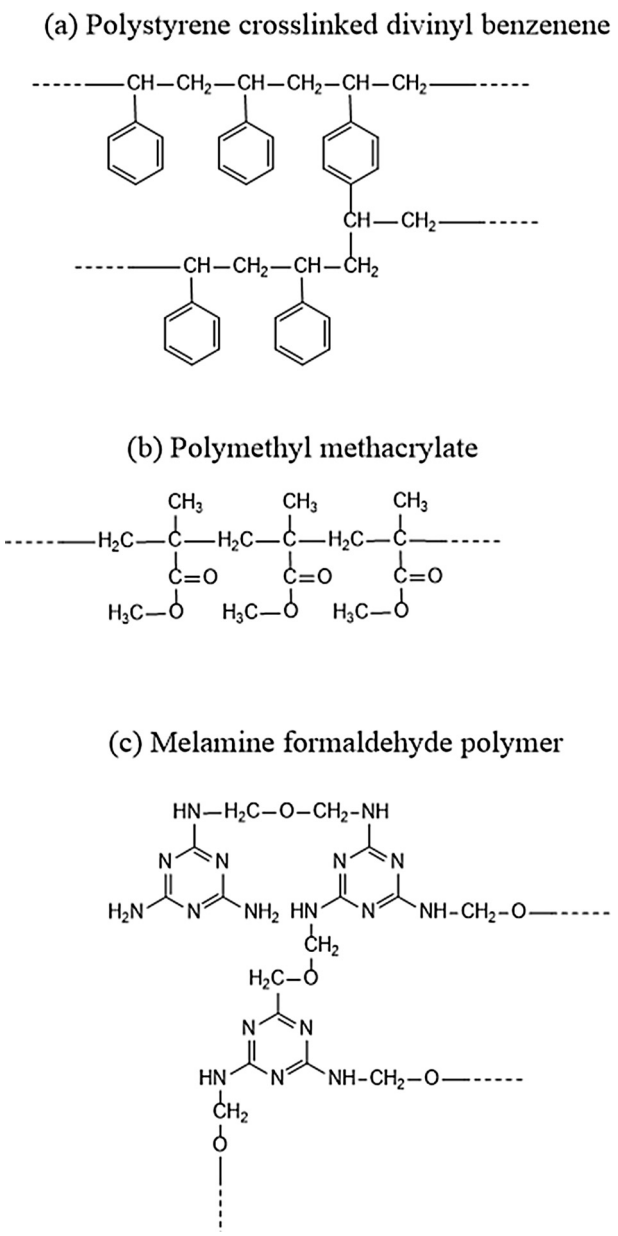

Fig. 4. The chemical structure of (a) polystyrene crosslinked divinyl benzene (PS-DVB) (b) polymethyl methacrylate (PMMA) and (c) Melamine formaldehyde polymer (MF).

penetrate deeply inside the structure of the PMMA/PCM26 aggregates to cover all the single microcapsules, thereby causing PMMA/PCM26 to adsorb more water.

3.1. MPCM-GPC density and porosity

The MPCM-GPC density and open porosity as a function of MPCM concentration are shown in Fig. 5. The addition of microcapsules can affect the porosity of the geopolymer concrete in several ways. For the same volume, the total surface area of small particles is much higher than for larger particles. Accordingly, more binder paste adsorbs to the surface of small particles. This can cause more voids between the particles (aggregates and microcapsules) [5]. This is counteracted by the cavity filling effect [31–33]. The cavity between aggregates and sand can be filled up by small particles ($\leq$125 μm) [33] causing an increase of the packing density, thereby reducing the porosity of the concrete. The single microcapsules have a small size in the range of 1–100 μm (Fig. 2). However, the effective size is larger due to agglomeration. The agglomerates of PS-DVB/RT27 and PMMA/PCM26 are too large to fill in the cavities in the concrete structure (Fig. 2a) [3,34–36]. Only MF/PCM24 with a much smaller size distribution (Fig. 2a) can fill up the cavities to reduce the porosity. In addition, the properties of the polymer shell can affect the porosity. As illustrated in Fig. 3, the hydrophobic PS-DVB/RT27 has little interaction with water. Accordingly, air gaps can be formed between the microcapsules and the geopolymer paste during the mixing process [5,37,38]. PMMA/PCM26 and MF/PCM24 have shells containing polar functional groups (Fig. 4), providing better interaction with the aqueous alkaline environment (Fig. 3). This results in better interface bonds between the microcapsules and the geopolymer paste, thereby reducing the air gaps between MPCM and geopolymer paste. The more polar functional groups on the polymer shell also helps to disperse the microcapsules into the concrete matrix better than a hydrophobic shell. This is evident in the SEM images (Fig. 6) which show obvious gaps between the concrete matrix and PS-DVB/RT27, while the polymers with polar functional groups exhibit almost no air gaps (PMMA/PCM26) or very small air gaps (MF/PCM24). The porosity of the concrete will be governed by a combination of these effects.

As can be seen from Fig. 5a, the open porosity increases with microcapsule concentration. This can be explained by the smaller size of the microcapsule agglomerates compared to sand (Fig. 2a), causing a larger surface area that adsorbs more binder paste to the surface. The D_{50} size of sand is approximately 4–5 times larger than the PS-DVB/RT27 and PMMA/PCM26 agglomerates and 30 times larger than MF/PCM24. When the concentration of MPCM is raised, the porosity of GPC with MF/PCM24 increases at a higher rate than PS-DVB/RT27 and PMMA/PCM26. This is probably due to the combination of the small size and the polar functional groups on the microcapsule shell, which causes MF/PCM24 to adsorb more binder paste. However, this is not consistent with the trapped water content (Fig. 3) where PMMA/PCM26 is shown to trap more water than MF/PCM24. This discrepancy might be due the high viscosity and short setting time of the geopolymer mixture, preventing the water to penetrate deeply into the PMMA/PCM26 agglomerates before the geopolymer sets. Accordingly, only the outer surface of the PMMA/PCM26 agglomerates are covered, reducing the amount of binder adsorption onto PMMA/PCM26. When more geopolymer paste is adsorbed onto the microcapsules, the viscosity increases and the probability of forming entrapped air voids during the mixing and pouring process is raised [5,7]. This is in agreement with the X-ray micro-tomography data (Fig. 7), which will be discussed in more details below.

The density of MPCM-GPC decreases when the MPCM concentration increases (Fig. 5b). This is due to the lower density of the microcapsules compared to the sand it replaces combined with the increase of the porosity. Similar observations have also been found previously [9,15].

3.2. Microstructure of MPCM-GPC

Fig. 6 shows the SEM images of geopolymer concrete with 2.6 wt% microcapsules. As is evident from Fig. 6b, the original PMMA/PCM26 agglomerates (Fig. 2b) are broken into smaller entities after mixing, resulting in a better dispersion of the single microcapsules. This indicates that the physical bonds holding the PMMA/PCM26 agglomerates together are relatively weak. It can be seen that PMMA/PCM26 and MF/PCM24 are well dispersed in the geopolymer concrete while the more hydrophobic PS-DVB/RT27 is not dispersed properly, as is evident from the presence of large irregular agglomerates. In addition, the SEM images reveal that the single microcapsules remain stable with a spherical shape in the concrete matrix. This demonstrates that the microcapsules can withstand the current mixing process of the concrete.

Fig. 7 presents X-ray micro-tomography cross-sectional slices obtained from GPC without MPCM and GPC containing 2.6 wt% of MPCM. In the X-ray micro-tomography images, the air bubbles and microcapsules are shown as dark colors due to low or no absorption of X-rays

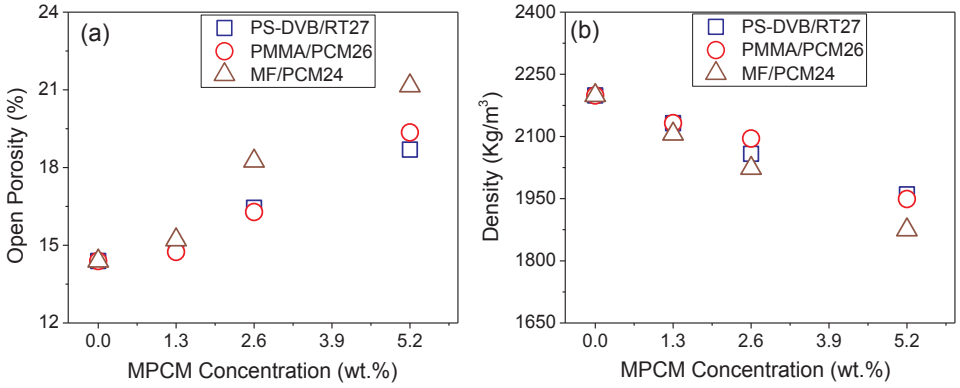

Fig. 5. Open porosity (a) and density (b) and of GPC at different MPCM concentrations.

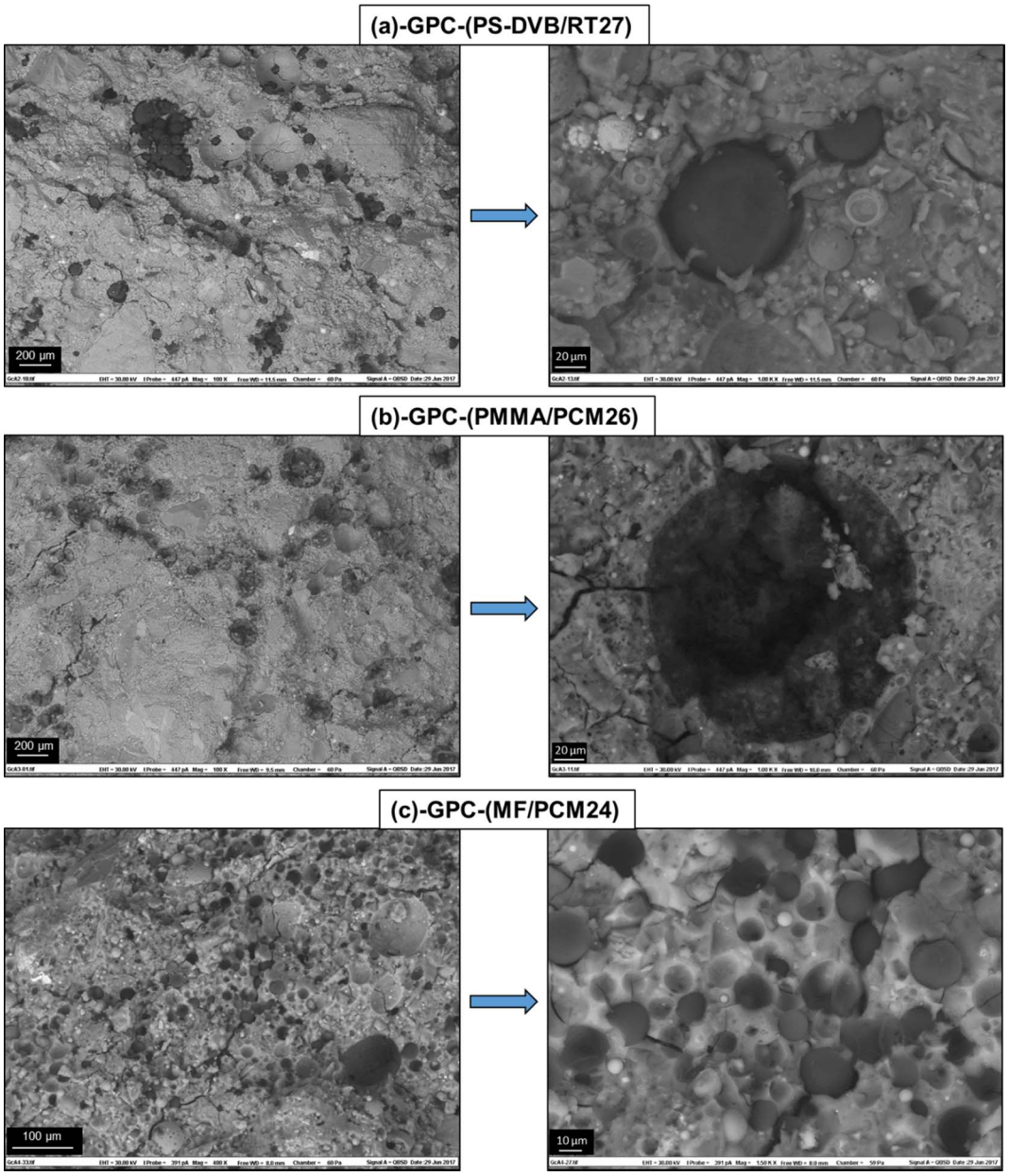

Fig. 6. SEM images of GPC containing 2.6 wt% of (a) PS-DVB/RT27, (b) PMMA/PCM26 and (c) MF/PCM24.

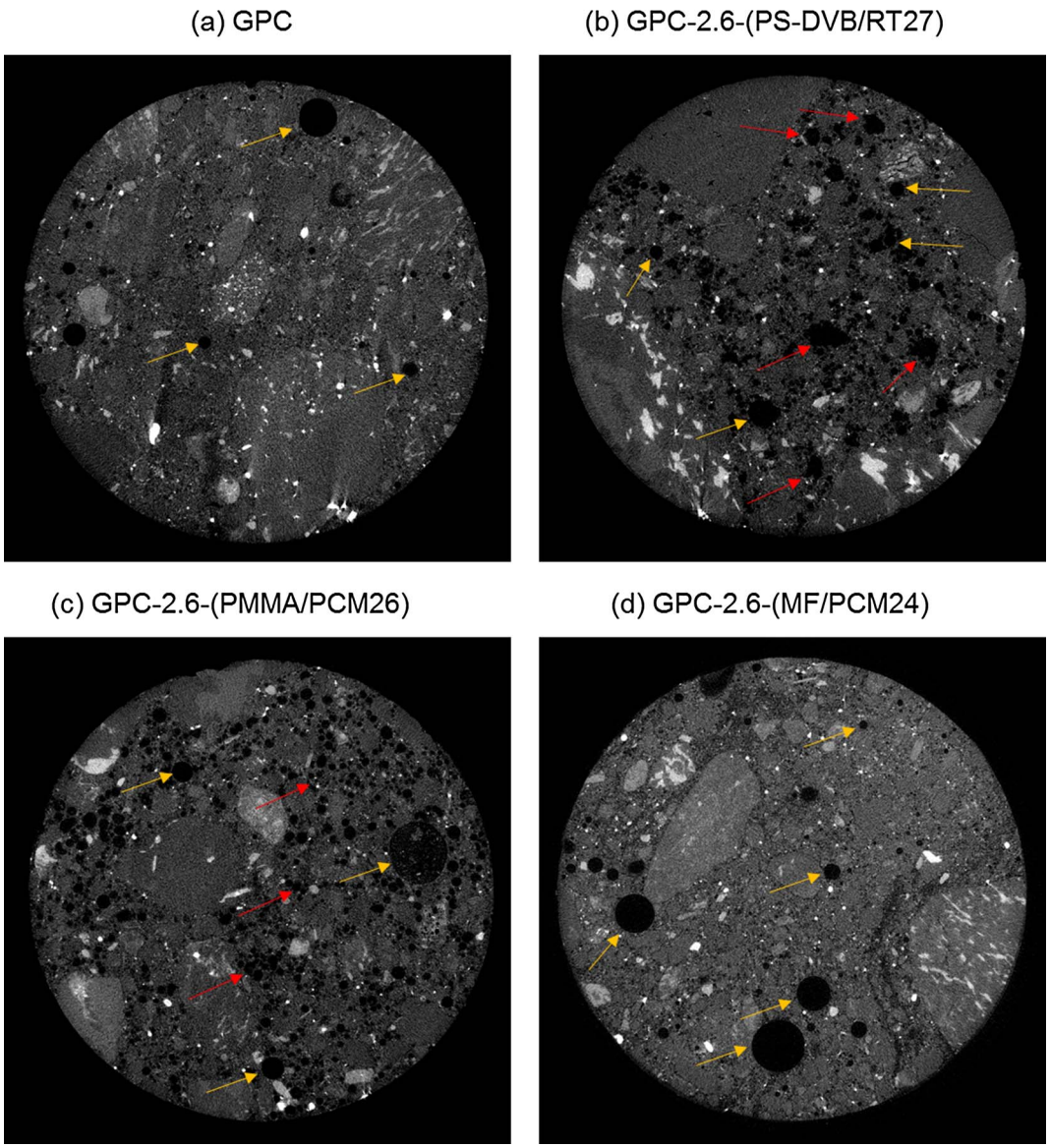

Fig. 7. X-ray-tomography images of (a) GPC without MPCM, (b) GPC containing 2.6 wt% PS-DVB/RT27, (c) GPC containing 2.6 wt% PMMA/PCM26 and (d) GPC containing 2.6 wt% MF/PCM24. The yellow arrows point the air bubbles and the red arrows indicate the microcapsules. The field of view is 1 cm. (For interpretation of the references to colour in this figure legend, the reader is referred to the web version of this article.)

while bright colors represent sand and gravel, which can adsorb high amounts of X-rays. The purpose of using X-ray micro-tomography is to investigate the internal microstructure of the concrete samples, and to evaluate how the microcapsules and the air bubbles are dispersed in the concrete matrix. This can provide important information for thermal and mechanical properties of concrete. It is difficult to discriminate between air bubbles and microcapsules based on grey scale values, due to the low level of X-ray attenuation of the organic materials constituting the MPCM [7]. However, air bubbles have tendency to be approximately spherical due to interfacial tension effects, while MPCM might exist as agglomerates with a more irregular shape [7]. For GPC containing PMMA/PCM26, it is difficult to distinguish air bubbles and MPCM based on the shape because the PMMA/PCM26 has a spherical aggregate structure (SEM, Fig. 6b). This is confirmed by Fig. 7c, where both MPCM and air bubbles appears in a spherical shape. However, some air bubbles can be distinguished (the yellow arrows) since the sizes are much larger than size distribution of PMMA/PCM26. For GPC containing MF/PCM24 (Fig. 7d), a high amount of spherical air bubbles can be observed (the yellow arrows) while the agglomerated microcapsules MF/PCM24 cannot be detected. The agglomerated microcapsules MF/PCM24 have a size of 21 μm (Fig. 2) which are too small to be easily visible in the X-ray tomography images. This illustrates that the MF/PCM24 microcapsules are well dispersed in GPC with no large agglomerates formed during the mixing process.

GPC containing the hydrophobic PS-DVB/RT27 microcapsules is different from GPC containing microcapsules with a polymer shell containing polar functional groups (PMMA/PCM26 and MF/PCM24). For PS-DVB/RT27, there is a clear difference between the spherical air bubbles and the irregular MPCM agglomerates (the yellow arrows and red arrows show air bubbles and MPCM, respectively). The presence of large agglomerates illustrates that PS-DVB/RT27 is not dispersed properly in the concrete matrix. A visual inspection of Fig. 7 show that the amount of air bubbles presented in GPC containing MF/PCM24 is higher than for the other samples. This is in agreement with the higher porosity of this sample (Fig. 5a).

3.3. Thermal properties of MPCM-GPC

The thermal conductivity of GPC containing MPCM (MPCM-GPC) at different temperatures (comparing the solid state and liquid states of

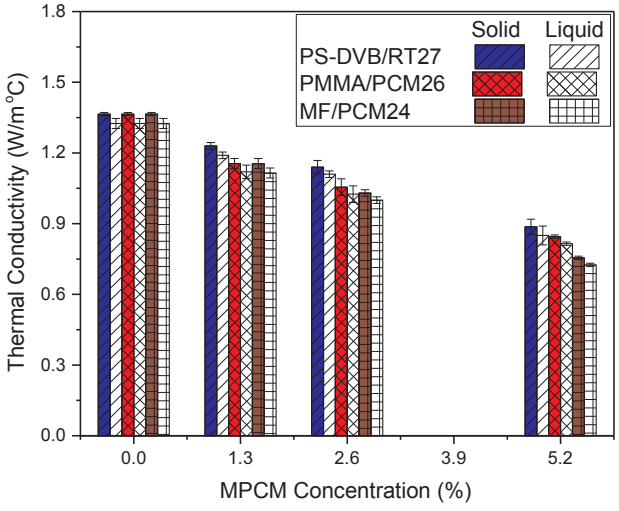

Fig. 8. Thermal conductivity of GPC containing microcapsules at the solid and liquid state of PCM as a function of microcapsule concentration.

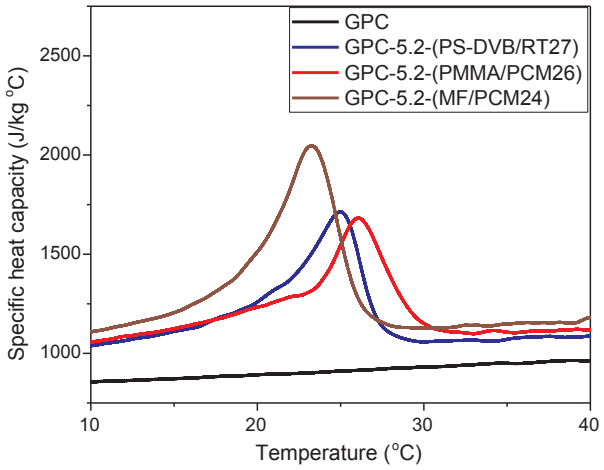

Fig. 9. The specific heat capacity as a function of temperature for GPC at 0 wt% and 5.2 wt% MPCM.

PCM) is summarized in Fig. 8. There is a clear reduction of the thermal conductivity of MPCM-GPC when the amount of microcapsules is increased. It is believed that the lower thermal conductivity of the microcapsules compared to that of replaced sand [5], the enhancement of porosity (Fig. 5a) and the poor interface between microcapsules and concrete matrix (Fig. 6) are the main reasons for the decline in thermal conductivity. The thermal conductivity of MPCM-GPC at low temperatures (5–10 °C) where PCM is in a solid state is slightly lower than at high temperatures (45–50 °C) where PCM is in a liquid state. The higher thermal conductivity of the solid PCM compared to the liquid PCM is a possible explanation [27,39]. However, since the difference between the thermal conductivity of MPCM-GPC for the solid PCM and liquid PCM is small, the average thermal conductivity will be used to calculate the thermal diffusivity of MPCM-GPC.

The reduction rates of thermal conductivity of GPC after mixing with different kinds of microcapsules are not significantly influenced by whether PCM is in a liquid or solid state. However, there is a slight difference between the different kinds of microcapsules, with reduction rates of 0.090, 0.096, 0.110 for GPC containing PS-DVB/RT27, PMMA/PCM26, MF/PCM24 respectively. Since air pores will reduce the thermal conductivity, the slightly different reduction rates are probably mostly due to the change in porosity (Fig. 5a). Furthermore, the smaller size and better distribution of MF/PCM24 compared to PS-DVB/RT27 and PMMA/PCM26 might contribute to this effect. A better distribution of microcapsules in the concrete matrix can increase the MPCM thermal pathway through concrete matrix thereby facilitating lower thermal conductivity. The thermal conductivity of each microcapsule might also play a role, but unfortunately, the thermal conductivity of the considered microcapsules is unknown.

Fig. 9 shows the specific heat capacity of GPC containing PS-DVB/RT27, PMMA/PCM26 and MF/PCM24 at a microcapsule concentration of 5.2 wt%. The specific heat capacity in the temperature range of 10–15 °C (below the melting range of PCM) and 35–40 °C (above melting range of PCM) were determined and is summarized in Fig. 10a.

As shown in Fig. 10a, for both liquid and solid PCMs the specific heat capacity of GPC increases slightly when the concentration of microcapsules is raised. This might be due to a lower specific heat capacity of geopolymer concrete compared to the microcapsules. In addition, there is almost no difference between the specific heat capacity of GPC containing microcapsules in the solid and liquid state of PCM (Fig. 10a). This observation is in good agreement with previous findings [5,29].

Fig. 10b summarizes the latent heat of GPC as a function of microcapsule concentration within the temperature range of 10–35 °C. The latent heat of concrete increases linearly when the microcapsule concentration is raised. MF/PCM24 increases fastest, with a slope (γ) of 0.93, while the lower slopes of PS-DVB/RT27 (γ = 0.70) and PMMA/PCM26 (γ = 0.73) are similar to each other. Several effects may cause γ to become lower than 1. A higher porosity of the concrete matrix might reduce γ [5]. However, this cannot explain the current results as MF/PCM24 exhibits the highest increase in open porosity (Fig. 5) and the largest γ. A possible reason for this discrepancy is that the gaps between the particles and the GPC matrix play an important role. MF/PCM24 exhibits very little gaps between the microcapsules and the GPC matrix, which will improve the heat transfer to the particles and increase γ. In addition, MF/PCM24 is well dispersed as single, small microcapsules while PS-DVB/RT27 and PMMA/PCM26 exist as agglomerates of approximately the same size as each other (Fig. 6). Agglomerated structures can impede the heat transfer to the single microcapsules, thereby reducing γ.

3.4. Thermal diffusivity

The calculated thermal diffusivity of GPC containing microcapsules (MPCM-GPC) are shown in Fig. 11. According to Fig. 11a, the thermal diffusivity of MPCM-GPC decreases with the concentration of microcapsules over the whole temperature range. Comparing the different microcapsules (Fig. 11b), the thermal diffusivity of GPC containing MF/PCM24 is lowest while GPC containing PMMA/PCM26 is slightly lower than that of PS-DVB/RT27. This is especially evident for the temperatures outside the melting range of the microcapsules. The lower thermal diffusivity of MF/PCM24 is probably related to the higher amount of air bubbles in this sample (the air will act as a thermal insulator), and the higher apparent heat capacity. The thermal diffusivity provides important information regarding the transient thermal conduction process through a wall. Materials with smaller thermal diffusivity can reduce the heat transfers through the wall, resulting a smaller effect of the outdoor environment on the indoor environment and cause a reduction in heating/cooling energy consumption to maintain the indoor temperature at the desired level. The results indicate that GPC containing MF/PCM24 can have better effect on reducing the heating/cooling energy consumption than PS-DVB/RT27 and PMMA/PCM26.

3.5. Energy saving

Fig. 12 presents the simulated indoor surface temperature, and the inner wall heat flux as a function of time and the total consumed power for heating and cooling of GPC containing 0 wt% and 5.2 wt% microcapsules.

The addition of microcapsules causes a higher heat storage capacity

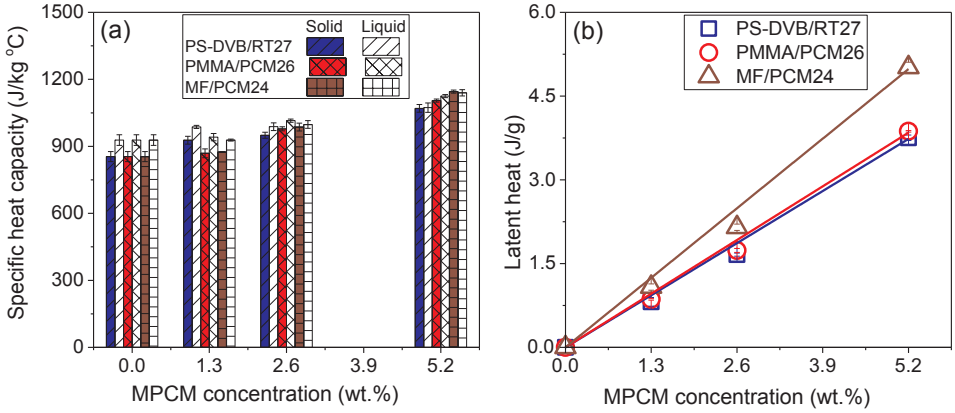

Fig. 10. (a) The specific heat capacity (b) the latent heat of GPC as a function of concentration of MPCM.

and lower thermal conductivity of the GPC samples, leading to a lower thermal diffusivity (Fig. 11). Accordingly, the heat transfers through the wall can be reduced, resulting in a smaller effect of the outdoor environment on the indoor temperature, and thereby causing a reduction in the energy consumption need to maintain the indoor temperature at 23 °C.

The effect of the PCM latent heat on the heat transfer process can be seen clearly as a slight transition point around the melting point of PCM for both the indoor surface temperature and the inner wall heat flux (Fig. 12a, b). This is especially evident for MF/PCM24. Similar observations were also found previously [3,27,35]. After adding 5.2 wt% of microcapsules to GPC, the variation of indoor surface temperature of the GPC is lower and closer to the human comfort zone than for pure GPC (0 wt%) (Fig. 12a). The microcapsules induce a lower heat transfer (heat flux) to the indoor side of the concrete wall (Fig. 12b). Accordingly, a lower power consumption is needed to maintain the indoor environment at the desired temperature (Fig. 12c). When utilizing 5.2 wt% of microcapsules, the total energy consumption for to maintain an indoor temperature of 23 °C is reduced by up to 18.5 ± 0.3% for PS-DVB/RT27, 20.1 ± 0.7% for PMMA/PCM26 and 25.9 ± 0.3% for MF/PCM24 (Fig. 12d). The higher energy saving potential of MF/PCM24 compared to PS-DVB/RT27 and PMMA/PCM26 can be explained by the formation of a structure with more insulating pores (higher porosity content) and the higher heat storage capacity of MF/PCM24. This is in agreement with the thermal diffusivity of GPC containing MPCM (Fig. 11).

3.6. Compressive strength

Fig. 13 presents the compressive strength of GPC containing microcapsules at 20 °C (below the microcapsule melting point) and 40 °C (above the microcapsule melting point) as a function of microcapsule concentration. The compressive strength of GPC declines significantly when the concentration of microcapsules increases for both states of PCM, in agreement with previous findings [3,5].

The compressive strength of GPC containing microcapsules follows the order of MF/PCM24 < PMMA/PCM26 < PS-DVB/RT27. This trend is more obvious at high microcapsule concentrations (≥ 2.6 wt%). The compressive strength of concrete will be lower when there are the more air voids (porosity) [3,5], softer particles [7] and poorer dispersion of particles in the concrete matrix [40,41]. Air gaps between microcapsules and concrete indicates poor interfacial bonds, which can result in a lower compressive strength [3,5,7]. Combination of these factors plays an important role regarding the effect of microcapsules on the compressive strength of geopolymer concrete. At high microcapsule concentrations, MF/PCM24 has a significantly lower compressive strength than the other samples even when the PCM is in a solid state. This might be due to the higher amounts of air bubbles in this sample and the higher core/shell ratio of MF/PCM24 which may result in softer particles.

Fig. 13a shows that the compressive strength of GPC containing microcapsules with PCM in a solid state is higher than when PCM is in a liquid state. This might be due to an increase of the internal stress of the microcapsules at elevated temperatures (due to thermal expansion). It is also possible that the microcapsules become softer when they have a liquid core. Fig. 13b shows the percentage reduction of the compressive strength of GPC containing microcapsules when PCM is changed from a solid to liquid state. The percentage reduction increases when the amount of microcapsules increases, confirming that the microcapsules are the cause of the decline in compressive strength. Furthermore,

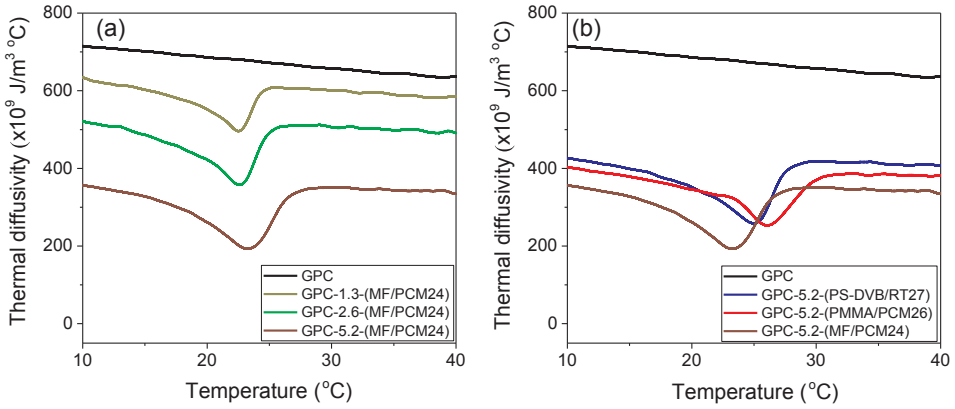

Fig. 11. Thermal diffusivity of (a) GPC containing different concentrations of MF/PCMPC24 and (b) GPC containing 5.2 wt% of PS-DVB/RT27, PMMA/PCM26 and MF/PCM24 as a function of temperature.

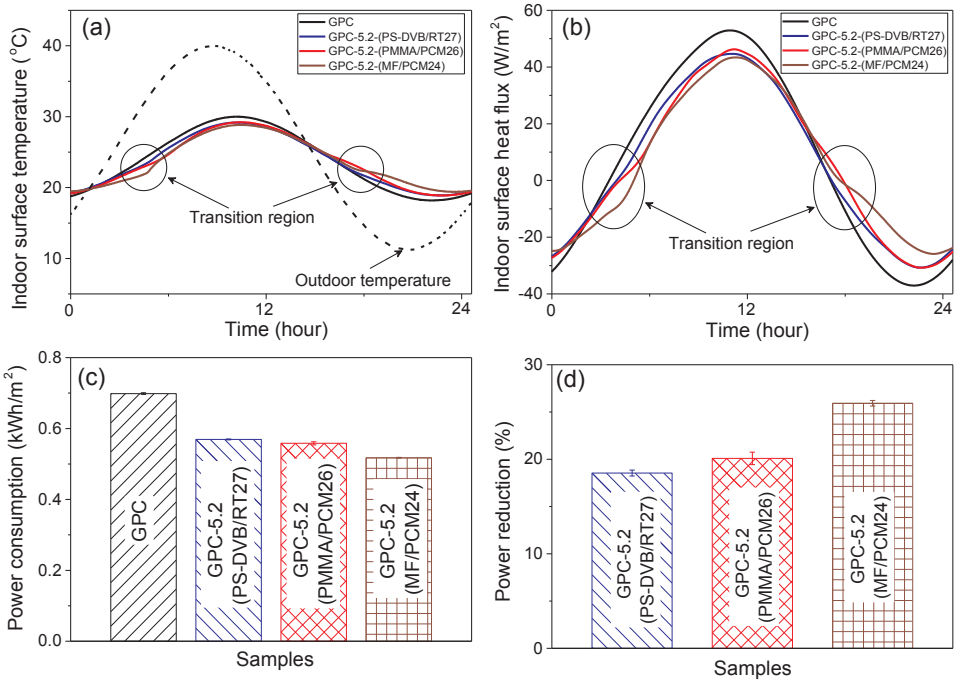

Fig. 12. (a) The simulated indoor surface temperature; (b) the simulated indoor surface heat flux through a 50 mm thick geopolymer concrete wall containing MPCM after exposing it to a sinusoidal outdoor temperature fluctuation (Eq. (8)); (c) the simulated power consumption for heating and cooling the system to maintain an indoor temperature of 23 °C and (d) the power reduction (%) after adding 5.2 wt% of MPCM compared to a corresponding sample without MPCM.

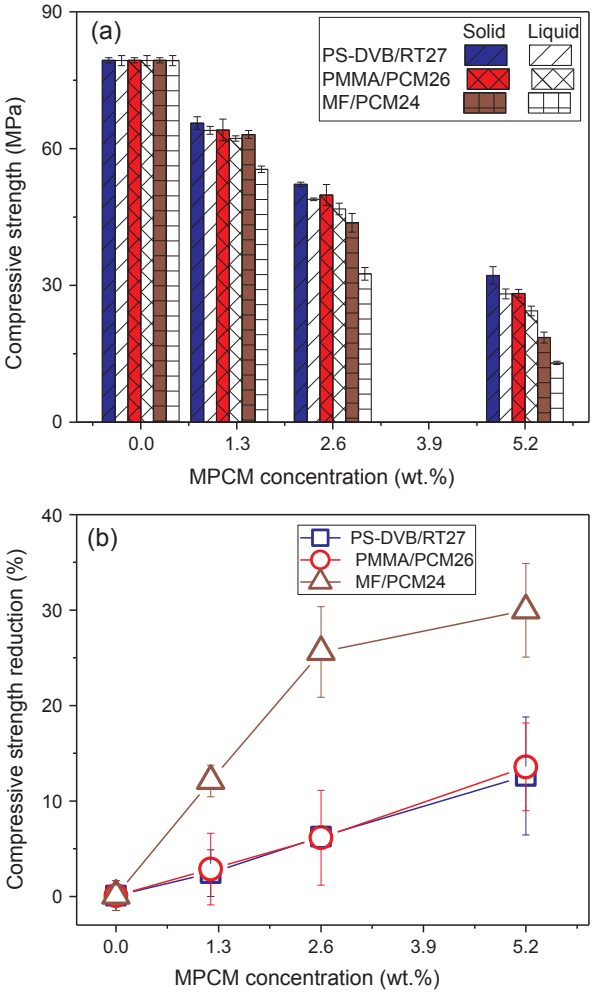

Fig. 13. (a) The compressive strength of GPC containing microcapsules below (20 °C) and above (40 °C) the melting range of PCM and (b) the compressive strength reduction between the solid and liquid state of PCM.

melting of the PCM core affects the MF/PCM24 much more than for PS-DVB/RT27 and PMMA/PCM26. This might be due to the higher paraffin core/polymer shell ratio of MF/PCM24 compared to PS-DVB/RT27 and PMMA/PCM26 (Table 1). In addition, the closer interface (lack of air gaps) between MF/PCM24 and concrete matrix facilitates better transfer of the compressive force to the microcapsules, and makes the concrete more sensitive to a possible thermal expansion of the microcapsules. However, PMMA/PCM26 also has a good interface with the concrete matrix. PMMA/PCM26 exists as agglomerates, which can contain voids between the microcapsules. Accordingly, there will be less stress on the microcapsules during compression and when they expand.

The compressive strength at 5.2% MPCM is 32 ± 2 MPa (solid state) and 28 ± 1 MPa (liquid sate) for PS-DVB/RT27 while for PMMA/PCM26 it is 28 ± 1 MPa (solid state) and 24 ± 1 MPa (liquid state). Accordingly, the integration of PS-DVB/RT27 and PMMA/PCM26 into GPC at 5.2 wt% satisfy the mechanical European regulation (EN 206-1, compressive strength class C20/25) for concrete for building construction. Unfortunately, while 5.2% of MF/PCM24 shows the best thermal performance, its compressive strength is only 19 ± 1 MPa (solid state) and 13.0 ± 0.4 MPa (liquid state), which does not satisfy the European regulation for compressive strength. Therefore, further investigations to improve the mechanical strength to satisfy the mechanical regulation is needed in order to utilize MF/PCM24 as a thermoregulation component in geopolymer concrete for building applications.

4. Conclusion

The integration of microencapsulated phase change materials (MPCM) into geopolymer concrete (GPC) was found to improve the thermal energy storage capacity, reduce the thermal conductivity and decrease the density, resulting in an enhancement of the energy efficiency. MF/PCM24 with a polymer shell containing polar functional groups, the highest core/shell ratio (9:1) and the smallest size (10–100 μm) exhibited the largest increase of GPC porosity, better interface bonds between microcapsules and the concrete matrix, and a more uniform dispersion in the concrete matrix compared to PS-DVB/RT27 and PMMA/PCM26. The reduction of power consumption for

stabilizing the indoor temperature at 23 °C was also highest for MF/PCM24 at 25.9 ± 0.3% utilizing 5.2 wt% microcapsules, while the corresponding values was 18.5 ± 0.3% for PS-DVB/RT27, and 20.1 ± 0.7% for PMMA/PCM26.

The main drawback of MPCM addition is the significant reduction of compressive strength, which is also more pronounced for MF/PCM24 due to the larger amount of air pockets and a higher core/shell ratio than PS-DVB/RT27 and PMMA/PCM26.

The compressive strength of GPC containing MPCM decreases when PCM changes from a solid to liquid state. The reduction is most pronounced for MF/PCM24, probably due to the lack of air gaps between MPCM and the GPC combined with a higher core/shell ratio.

The addition of PS-DVB/RT27 and PMMA/PCM26 to GPC was found to satisfy the demand of mechanical properties for structural applications. MF/PCM24 was found to be the best choice for saving energy, but unfortunately the mechanical strength is too low. This challenge needs to be overcome in order to facilitate utilization in building materials.

Acknowledgement

We gratefully acknowledge funding from the Research Council of Norway, project number 238198. The authors gratefully acknowledge Rino Nilsen, Trond Atle Drøbak at Østfold University College and Van Thi Ai Nguyen for their assistance with laboratory work.

References

[1] E.P. EU Directive 2002/91/EC. Brussels; 2003.
[2] E.P. EU Directive 2010/31/UE. Strasburg; 2010.
[3] Hunger AGEM, Mandilaras I, Brouwers HJH, Founti M. The behavior of self-compacting concrete containing micro-encapsulated Phase Change Materials. Cem Concr Compos 2009;31:731–43.
[4] María Fenollera JLM, Goicoechea Itziar, Lorenzo Jaime, Álvarez Miguel Ángel. The influence of phase change materials on the properties of self-compacting concrete. Materials 2013;6:3530–46.
[5] Cao VD, Pilehvar S, Salas-Bringas C, Szczotok AM, Rodriguez JF, Carmona M, et al. Microencapsulated phase change materials for enhancing the thermal performance of Portland cement concrete and geopolymer concrete for passive building applications. Energy Convers Manage 2017;133:56–66.
[6] Eddhahak-Ouni A, Drissi S, Colin J, Neji J, Care S. Experimental and multi-scale analysis of the thermal properties of Portland cement concretes embedded with microencapsulated Phase Change Materials (PCMs). Appl Therm Eng 2014;64:32–9.
[7] Pilehvar S, Cao VD, Szczotok AM, Valentini L, Salvioni D, Magistri M, et al. Mechanical properties and microscale changes of geopolymer concrete and Portland cement concrete containing micro-encapsulated phase change materials. Cem Concr Res 2017;100:341–9.
[8] Pisello AL, D'Alessandro A, Fabiani C, Fiorelli AP, Ubertini F, Cabeza LF, et al. Multifunctional analysis of innovative PCM-filled concretes. Energy Procedia 2017;111:81–90.
[9] Wei Z, Falzone G, Wang B, Thiele A, Puerta-Falla G, Pilon L, et al. The durability of cementitious composites containing microencapsulated phase change materials. Cem Concr Compos 2017;81:66–76.
[10] Benhelal E, Zahedi G, Shamsaei E, Bahadori A. Global strategies and potentials to curb CO_2 emissions in cement industry. J Cleaner Prod 2013;51:142–61.
[11] Duxson P, Fernandez-Jimenez A, Provis JL, Lukey GC, Palomo A, Deventer JSJv. Geopolymer technology: the current state of the art. J Mater Sci 2007;42:2917–33.
[12] Zuhua Z, Xiao Y, Huajun Z, Yue C. Role of water in the synthesis of calcined kaolin-based geopolymer. Appl Clay Sci 2009;43:218–23.
[13] Nematollahi B, Ranade R, Sanjayan J, Ramakrishnan S. Thermal and mechanical properties of sustainable lightweight strain hardening geopolymer composites. Arch Civil Mech Eng 2017;17:55–64.
[14] Nematollahi B, Sanjayan J, Shaikh FUA. Synthesis of heat and ambient cured one-part geopolymer mixes with different grades of sodium silicate. Ceram Int 2015;41:5696–704.
[15] Szczotok AM, Carmona M, Kjøniksen A-L, Rodriguez JF. Equilibrium adsorption of polyvinylpyrrolidone and its role on thermoregulating microcapsules synthesis process. Colloid Polym Sci 2017;40:4061–71.
[16] http://www.micronal.de. datasheet of DS-5038X.
[17] http://www.microteklabs.com/data-sheets.html. Data sheet of MPCM24D.
[18] Cao VD, Pilehvar S, Salas-Bringas C, Szczotok AM, Valentini L, Carmona M, et al. Influence of microcapsule size and shell polarity on thermal and mechanical properties of thermoregulating geopolymer concrete for passive building applications. Energy Convers Manage-Data Brief 2018.
[19] Pilehvar S, Cao VD, Szczotok AM, Carmona M, Valentini L, Lanzon M, et al. Physical and mechanical properties of fly ash/slag geopolymer concrete containing different types of micro-encapsulated phase change materials; 2018 [Submitted for publication].
[20] Nematollahi B, Sanjayan J. Efficacy of available superplasticizers on geopolymers. Res J Appl Sci Eng Technol 2014;7:1278–82.
[21] Nematollahi B, Sanjayan J. Effect of different superplasticizers and activator combinations on workability and strength of fly ash based geopolymer. Mater Des 2014;57:667–72.
[22] Jang JG, Lee NK, Lee HK. Fresh and hardened properties of alkali-activated fly ash/slag pastes with superplasticizers. Constr Build Mater 2014;50:169–76.
[23] Feldkamp LA, Davis LC, Kress JW. Practical cone-beam algorithm. J Opt Soc Am A 1984;1:612–9.
[24] Standard BS EN 12390–7. Testing hardened concrete. Part 7: Density of hardened concrete; 2009.
[25] Liu MYJ, Alengaram UJ, Jumaat MZ, Mo KH. Evaluation of thermal conductivity, mechanical and transportproperties of lightweight aggregate foamed geopolymer concrete. Energy Build 2014;72:238–45.
[26] Safiuddin M, Hearn N. Comparison of ASTM saturation techniques for measuring the permeable porosity of concrete. Cem Concr Res 2005;35:1008–13.
[27] Cui H, Liao W, Mi X, Lo TY, Chen D. Study on functional and mechanical properties of cement mortar with graphite-modified microencapsulated phase-change materials. Energy Build 2015;105:273–84.
[28] Tittelein P, Gibout S, Franquet E, Johannes K, Zalewski L, Kuznik F, et al. Simulation of the thermal and energy behaviour of a composite material containing encapsulated-PCM: influence of the thermodynamical modelling. Appl Energy 2015;140:269–74.
[29] Joulin A, Zalewski L, Lassue S, Naji H. Experimental investigation of thermal characteristics of a mortar with or without a micro-encapsulated phase change material. Appl Therm Eng 2014;66:171–80.
[30] Cengel YA. Heat transfer: a practical approach. 2nd ed. Mcgraw-Hill; 2002.
[31] Mucteba U, Kemalettin Y. Effect of mineral admixtures on properties of self-compacting concrete. Cem Concr Compos 2011;33:771–6.
[32] Nikbin IM, Beygi MHA, Kazemi MT, Vaseghi Amiri J, Rabbanifar S, Rahmani E, et al. A comprehensive investigation into the effect of water to cement ratio and powder content on mechanical properties of self-compacting concrete. Constr Build Mater 2014;57:69–80.
[33] Chad Norvell DJS, Dusicka Peter. The effect of microencapsulated phase-change material on the compressive strength of structural concrete. J Green Build 2013;8:116–24.
[34] Dehdezi PK, Hall MR, Dawson AR, Casey SP. Thermal, mechanical and microstructural analysis of concrete containing microencapsulated phase change materials. Int J Pavement Eng 2012;14:449–62.
[35] Borreguero AM, Serrano A, Garrido I, Rodríguez JF, Carmona M. Polymeric-SiO_2-PCMs for improving the thermal properties of gypsum applied in energy efficient buildings. Energy Convers Manage 2014;87:138–44.
[36] Moosberg-Bustnes H, Lagerblad B, Forssberg E. The function of fillers in concrete. Mater Struct 2004;37:74–81.
[37] Fedroff D, Ahmad S, Savas B. Mechanical properties of concrete with ground waste tire rubber. Transpor Res Board 1996;1532:66–72.
[38] Khatib ZK, Bayomy FM. Rubberized Portland cement concrete. J Mater Civ Eng 1999;11:206–13.
[39] Ukrainczyk SKN, Šipušiæ J. Thermophysical comparison of five commercial paraffin waxes as latent heat storage materials. Chem Biochem Eng Q 2010;24:129–37.
[40] Vahedi F, Shahverdi HR, Shokrieh MM, Esmkhani M. Effects of carbon nanotube content on the mechanical and electrical properties of epoxy-based composites. New Carbon Mater 2014;29:419–25.
[41] Elkady H, Serag MI, Elfeky MS. Effect of nano silica de-agglomeration, and methods of adding super-plasticizer on the compressive strength, and workability of nano silica concrete. Civil Environ Res 2013;3:21–34.